

# CGPart: A Part Segmentation Dataset Based on 3D Computer Graphics Models

Qing Liu<sup>1</sup>, Adam Kortylewski<sup>1</sup>, Zhishuai Zhang<sup>1</sup>, Zizhang Li<sup>2\*</sup>  
 Mengqi Guo<sup>3\*</sup>, Qihao Liu<sup>1</sup>, Xiaoding Yuan<sup>4\*</sup>, Jiteng Mu<sup>5\*</sup>, Weichao Qiu<sup>1</sup>, Alan Yuille<sup>1</sup>  
<sup>1</sup>Johns Hopkins University <sup>2</sup>Zhejiang University  
<sup>3</sup>Beihang University <sup>4</sup>Tongji University <sup>5</sup>University of California, San Diego

qingliu@jhu.edu, akortyl1@jhu.edu, zhshuai.zhang@gmail.com, zzli@zju.edu.cn  
 im.guomengqi@gmail.com, qliu45@jhu.edu, xiaodingyuan.tj@gmail.com, jmu@ucsd.edu  
 qiuwch@gmail.com, alan.l.yuille@gmail.com

## Abstract

Part segmentations provide a rich and detailed part-level description of objects, but their annotation requires an enormous amount of work. In this paper, we introduce CGPart, a comprehensive part segmentation dataset that provides detailed annotations on 3D CAD models, synthetic images, and real test images. CGPart includes 21 3D CAD models covering 5 vehicle categories, each with detailed per-mesh part labeling. The average number of parts per category is 24, which is larger than any existing datasets for part segmentation on vehicle objects. By varying the rendering parameters, we make 168,000 synthetic images from these CAD models, each with automatically generated part segmentation ground-truth. We also annotate part segmentations on 200 real images for evaluation purposes. To illustrate the value of CGPart, we apply it to image part segmentation through unsupervised domain adaptation (UDA). We evaluate several baseline methods by adapting top-performing UDA algorithms from related tasks to part segmentation. Moreover, we introduce a new method called Geometric-Matching Guided domain adaptation (GMG), which leverages the spatial object structure to guide the knowledge transfer from the synthetic to the real images. Experimental results demonstrate the advantage of our new algorithm and reveal insights for future improvement. We will release our data and code.

## 1. Introduction

Part-based object representations are of key importance for many computer vision tasks such as object recognition [108, 9, 77, 1], pose estimation [32, 101, 14, 104], action detection [93], and scene understanding [70, 81, 75]. Currently, part-based approaches often represent objects as a set of sparse keypoints, because these are easy to annotate in large-scale datasets for training deep neural networks. In contrast to keypoints, part segmentations provide a richer

and more detailed part-level object description, but require a much greater annotation effort. Therefore, part segmentation datasets mostly focus on a single object category, such as humans [20, 21, 46, 102] and faces [41, 32, 40], contain only a small number of images [9], or only define a small number of parts per object category [105]. These limitations have largely impeded the development of computer vision models that leverage part segmentations.

In this work, we introduce CGPart, a part segmentation dataset based on 3D computer graphics models (Figure 1). CGPart is composed of 21 3D CAD models from 5 vehicle categories. For each category, we define a fine-grained set of parts which are consistently annotated across all CAD models of the corresponding category. These detailedly labeled parts could provide useful information for various tasks. For example, the segmentation of parts such as *trunk* and *door* defined in *car* can be very useful for action recognition. Quantitatively, the average number of parts per category is 24, which is larger than any existing part segmentation dataset on vehicle objects. Based on the CAD models and their part annotations, we render a large-scale synthetic image dataset with automatically generated part segmentation ground-truth. These synthetic data could be used to train deep neural networks or test existing models for diagnostic purposes. Moreover, to facilitate studies targeting real-world data applications, CGPart provides carefully labeled part segmentations on 200 real images for evaluation purposes. In summary, CGPart is a large-scale part segmentation dataset that provides detailed annotations on 3D CAD models, synthetic images, and real test images.

To illustrate the value of CGPart, we use it as a new benchmark for unsupervised domain adaptation (UDA) for part segmentation. CGPart synthetic samples provide a large training set in the synthetic data domain, while its real images serve as a sufficient test set in the real data domain. In our experiments, we evaluate several baseline methods by adapting popular UDA approaches from related tasks to

\*This work is done during internship at Johns Hopkins University.

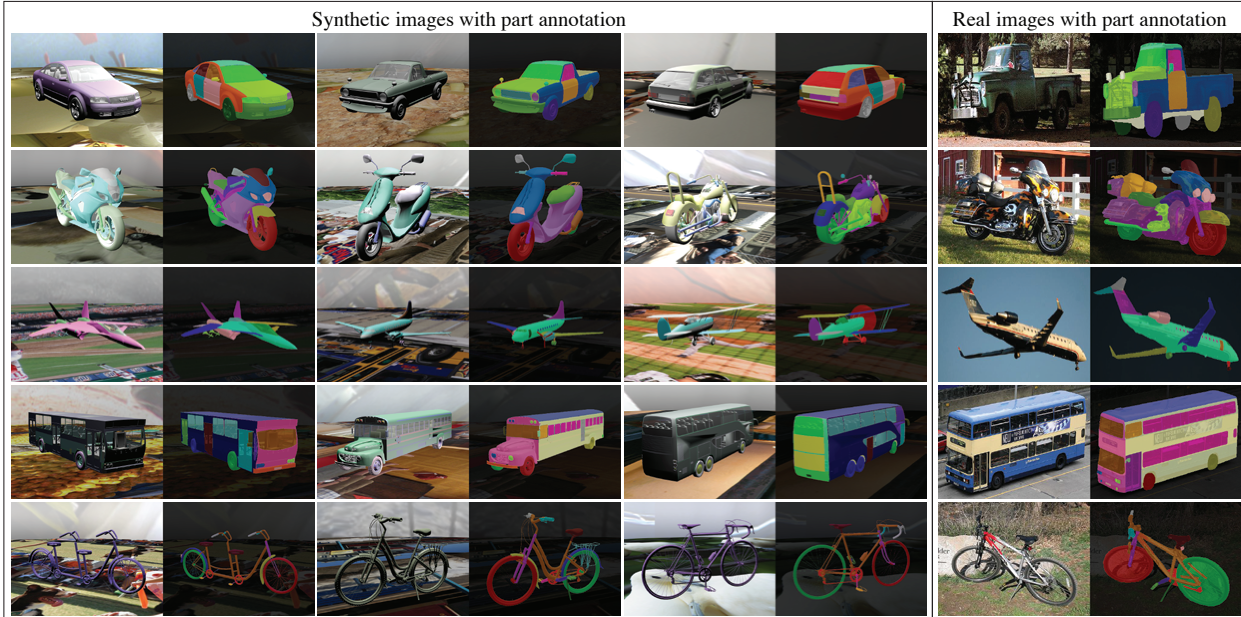


Figure 1: An overview of our CGPart dataset. CGPart is a new part segmentation dataset that provides detailed annotations on 3D CAD models, synthetic images, and real images. In particular, the dataset consists of five vehicle categories with several prototypes for each category, as shown in each row, and is composed of synthetic images with automatically generated segmentation ground-truth (left panel), as well as real test images with manually labeled part segmentations (right panel).

part segmentation. They outperform a naïve approach, and we analyze their pros and cons in detail.

Moreover, we introduce a novel algorithm called Geometric-Matching Guided domain adaptation (GMG), which conducts cross-domain geometric matching based on a geometric warping between real and synthetic images. Once an optimal match is found, GMG transfers the synthetic labels to the real images and retains the high-confidence results as pseudo-labels for a joint training process. In short, GMG explicitly uses the object structure depicted in the synthetic samples to guide the part segmentation on the real images. In our experiments, GMG outperforms all baseline methods on the CGPart real test data and the PascalPart dataset [9].

In summary, our main contributions are:

1. We introduce a new part segmentation dataset that provides detailed annotations on 3D CAD models, synthetic images, and real test images, and we apply it to part segmentation through unsupervised domain adaptation.
2. We implement and test several baseline approaches for unsupervised domain adaptation and find that they perform better than a naïve approach, but the results are still unsatisfactory.
3. We introduce a new method for unsupervised domain adaptation in part segmentation which leverages cross-domain geometric matching to transfer knowledge from synthetic to real and outperforms all baselines.

## 2. Related Work

**Datasets with part annotations of rigid objects.** There are multiple ways of annotating object parts in images. Bounding box and keypoint labels are relatively easy to obtain, while annotating pixel-level part segmentations is much more time-consuming. ImageNetPart [91] provides dense bounding box annotation for parts on 6 vehicle categories. PASCAL3D+ [101] includes keypoint annotation on 12 rigid object categories. CarFusion [65] and Apollo-Car3D [73] contain keypoint annotation for cars in street scenes. For 3D object part recognition, PartNet [57] provides hierarchical part annotations on 3D models covering 24 object categories, most of which are indoor furniture and none is a vehicle. Yi et al. [105] label parts on 3D models selected from 16 categories in ShapeNetCore [5], while their definition of part is coarse and the average number of parts per category is less than 4. In the context of image part segmentation, PascalPart [9] has been widely studied. It includes 20 categories for both rigid and non-rigid objects, but its average number of training samples and average number of annotated parts per category are small. An earlier dataset ETHZ [79] provides annotations of 5 parts on 141 wheelchair images and 6 parts on 139 car images, which is not adequate for deep network training. The lack of large-scale part segmentation on generic objects motivates our work on building a new dataset using 3D computer graphics models.

**Part segmentation.** Both rigid [74, 54] and non-rigid objects [20, 46, 90, 102] have been studied in part segmen-

tation, where structure-based methods, e.g., compositional models, are widely used [99, 100, 92, 90, 54]. Architecture-wise, both fully convolutional network (FCN) [98, 92] and long short-term memory (LSTM) [45, 47] have been studied. Many works explore the use of auxiliary tasks, especially pose estimation, to boost part segmentation and get promising results [18, 60, 99, 21]. Moreover, 3D information such as 3D geometric features [74] and depth [71] could also be embedded into the models to improve their performance. Recently, multi-object parsing is proposed and explored using graph matching [56] and boundary-semantic aware methods [111]. All of these methods are fully-supervised and require pixel-level annotations on real images. In this work, we explore UDA approaches which do not require annotations on real images for training.

**Learning from synthetic data.** Synthetic data generated by computer graphics techniques have many unique advantages. They are effective for model diagnosis [29, 110] and have boosted performance in many real-world application domains [58, 39, 64, 82, 87, 19, 24, 16]. However, the domain shift between synthetic data and real-world data limits the improvement. To overcome this, domain adaptation is proposed [63]. A major idea in domain adaptation is to learn domain-invariant representations by reducing the difference between source and target domain distributions. For example, Maximum Mean Discrepancy (MMD) and its kernel variants [76, 84, 52, 85] have been studied for this purpose. In the context of unsupervised domain adaptation (UDA) for semantic segmentation, self-training is one of the mainstream research directions [112, 113, 109, 42]. There has also been an increasing interest in using style transfer [59, 69, 25, 97, 44, 6] or feature alignment [26, 83] to encourage domain-wise marginal distribution matching. Other methods adopt category-aware feature alignment or local contextual feature similarity [55, 109, 15, 27]. Using extra information in the source domain, such as depth, has also been proven useful for UDA [10, 89]. In this work, we promote the idea of using UDA to solve part segmentation and guiding the knowledge transfer from synthetic to real based on the object structure.

**Image matching & geometric matching.** Image matching is an important research topic in object recognition and has many practical applications in image retrieval [107, 43, 31], one-shot learning [4, 88, 38], and geo-localization [80, 48, 106]. In cross-domain image matching, most recent works focus on learning domain-invariant feature representations [51, 37, 80, 48] based on Siamese network [11], and the matching is at image level. Geometric matching aims at finding spatial correspondences among images belonging to the same category at a more fine-grained level. Both hand-engineered descriptors [33, 49, 3] and pre-trained convolutional neural network (CNN) features [22, 86, 103, 78] are explored in early works. Recent progress is made in

trainable image descriptors [61, 35, 34] and trainable geometric models [7, 68, 67, 23]. However, these methods usually require either strong supervision in the form of ground-truth correspondences or weak supervision in matching image pairs. Moreover, they have only explored geometric matching for images in the same domain. Recently, Bai et al. [2] demonstrate that pre-trained CNN features can be effectively used to find spatial correspondence between synthetic images and real images. However, they do not combine it with a geometric transformation function nor consider dense correspondence. In this work, we explore cross-domain geometric matching without supervision and integrate it into our part segmentation framework.

### 3. The CGPart Dataset

In this section, we introduce CGPart, which is a part segmentation dataset based on 3D computer graphics models. CGPart is composed of 3D CAD models from 5 vehicle categories: *car*, *motorbike*, *aeroplane*, *bus*, and *bicycle*. We carefully per-mesh part labeling on the CAD models so they can be used to render a large-scale synthetic dataset with automatically generated part segmentation ground-truth.

#### 3.1. Data Generation

There are several criteria that our new benchmark needs to satisfy. First, the part labels should be fine-grained, i.e., the number of parts per category should be large. This ensures the models trained on our data will be useful in different problem settings. Second, we need to consider multiple prototypes (i.e., subtypes) for each object category to capture the intra-category variability and reduce the domain gap. Finally, an adequate number of real images needs to be annotated for evaluation purposes, such that we can benchmark the transfer to real-world scenarios. With the above criteria in mind, we construct CGPart in the following steps:

(1) **Select the 3D CAD models.** For each category, we select 4 to 5 high-quality 3D CAD models from ShapeNet-Core [5]. Each CAD model represents a common prototype (i.e., subtype) of the category it belongs to. For example, for the category *bicycle*, the CAD models are different bicycle subtypes such as *utility*, *sports*, *road*, and *tandem*. These can effectively represent the structural variability of bicycle objects. In total, we select 21 CAD models to be included and annotated in CGPart. A full list of these CAD models and their visualizations are included in the supplementary.

(2) **Define the list of parts to be studied.** We take references from existing vehicle part datasets [9, 79] and Wikipedia [95, 96, 94] to determine the part list for each category. Comparing with the part list in PascalPart [9], we make more fine-grained level definitions. For example, in PascalPart, the category *car* has a part “back side”. We instead distinguish “back windshield”, “tail light”, “back bumper”, and “trunk”. We also distinguish parts based on their relative positions. For example, “left handle” and

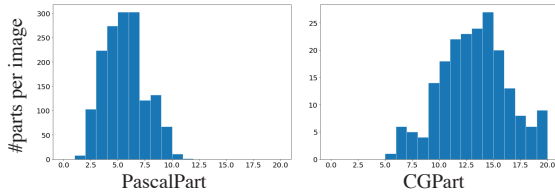


Figure 2: Histogram of number of parts per image in PascalPart [9] test split and CGPart real test images.

“right handle” are two different parts in *bicycle*, which implicitly requires the model to have a more comprehensive understanding of the object pose. Note that the fine-grained definition used here makes it possible to merge the part list and map to other coarse lists defined in existing datasets.

**(3) Annotate the parts on 3D CAD models.** We adopt the Blender [12] plugin built by Kim et al. [36] to perform per-mesh part labeling on the 3D CAD models. The plugin allows the user to assign a label to a group of selected meshes and save the results to a JSON file. We also add some support functions to the plugin, such as “show/hide selected from json”, or “colorize parts from json”. A screenshot of the software interface is shown in the supplementary. The plugin is also available in our public code base.

**(4) Render synthetic images with part annotations.** We use Blender [12] as our renderer to generate the synthetic images with part segmentation ground-truth. Following previous work [64, 82], we randomize the render parameters, including lighting, background, object texture, and viewpoint, to enable nuisance factor control and facilitate domain generalization. We generate 8000 synthetic images with resolution  $2048 \times 1024$  for each 3D CAD model and split the training and test set with a ratio of 3 : 1, resulting in a total of 126000 images for training and 42000 for testing. Example images with segmentation ground-truth are shown in the left panel of Figure 1.

**(5) Annotate the parts on real test images.** We manually label part segmentations on 200 real vehicle images (40 images per category) for evaluation purposes. The images are selected from PASCAL3D+ dataset [101] to contain high-resolution and non-occluded objects from various subtypes and evenly distributed viewpoints. We use the VGG Image Annotator (VIA) [17] to label the parts on the images. Example real images with annotation results are shown in the right panel of Figure 1. A screenshot of the annotator interface is also included in the supplementary.

### 3.2. Dataset Comparison

In Table 1, we compare CGPart with existing datasets that have vehicle part segmentation annotations. CGPart contains the largest number of parts per category, and its annotation on both synthetic images and real images makes it useful for various studies, e.g., unsupervised domain adaptation. In Figure 2, we compare the number of parts per image labeled on PascalPart and CGPart real test images. Generally, CGPart contains 2 to 3 times more annotations per

	CGPart (Ours)	PascalPart [9]	ETHZ [79]	SNPart [105]
3D Models	✓	✗	✗	✓
Syn. Img.	✓	✗	✗	✗
Real Img.	✓	✓	✓	✗
Avg. #Parts per Cat.	24	9	6	4

Table 1: Comparison of CGPart with existing datasets that have part segmentation annotations on vehicles.

image, making it a challenging part segmentation benchmark. More comprehensive comparisons between CGPart and PascalPart can be found in the supplementary material. In conclusion, CGPart is the first large-scale part segmentation dataset that provides detailed annotations on 3D CAD models, synthetic images, and real test images.

## 4. Geometric-Matching Guided Adaptation

To illustrate the value of CGPart, we apply it to image part segmentation through unsupervised domain adaptation (UDA) and propose a new algorithm for this task. In this section, we introduce our proposed Geometric-Matching Guided domain adaptation (GMG) approach. The key steps of GMG are illustrated in Figure 3 and will be discussed in detail in the following.

### 4.1. Preliminaries for Part Segmentation and UDA

We start with the preliminaries for part segmentation and unsupervised domain adaptation (UDA). In our work and all baseline experiments, we assume the category label is known, such that the part segmentation models are trained and tested for each object category separately. This assumption is reasonable since many off-the-shelf classifiers are freely available for the vehicle objects included in CGPart.

Similar to semantic segmentation, a part segmentation model  $\mathbf{M}$  can be formulated as a mapping function from the image domain to the output label domain:  $\mathbf{M} : I \rightarrow Y$ , which predicts a pixel-wise category label  $Y \in \{1, \dots, C\}^{H \times W}$ , where  $H$  and  $W$  denote the image size,  $C$  is the total number of part categories.

In UDA, the data are usually collected from two domains: source domain  $\mathcal{S}$  (i.e., synthetic data) and target domain  $\mathcal{T}$  (i.e., real data). During training, we have access to the labeled training samples  $(I^s, Y^s)$  from  $\mathcal{S}_{\text{train}}$  and unlabeled training samples  $I^t$  from  $\mathcal{T}_{\text{train}}$ . The goal is to train a model  $\mathbf{M}$  that can predict accurately on the test samples in  $\mathcal{T}_{\text{test}}$ . Most existing approaches start with training a *Source-Only* model  $\mathbf{M}^s$  on the labeled source data. For segmentation models with softmax output, the cross-entropy loss is widely used during the optimization process:

$$\mathcal{L}_{ce}(I^s, Y^s) = - \sum_{i=1}^H \sum_{j=1}^W \sum_{c=1}^C y_{(i,j),c}^s \log p_{(i,j)}(c|I^s; \mathbf{w}),$$

where  $(i, j)$  are the pixel coordinates in  $I^s$ ,  $c$  is the category index,  $y_{(i,j),c}^s \in \{0, 1\}$  is entry in the one-hot vector of the ground-truth label, i.e.,  $\forall(i, j), \sum_c y_{(i,j),c}^s = 1$ , and

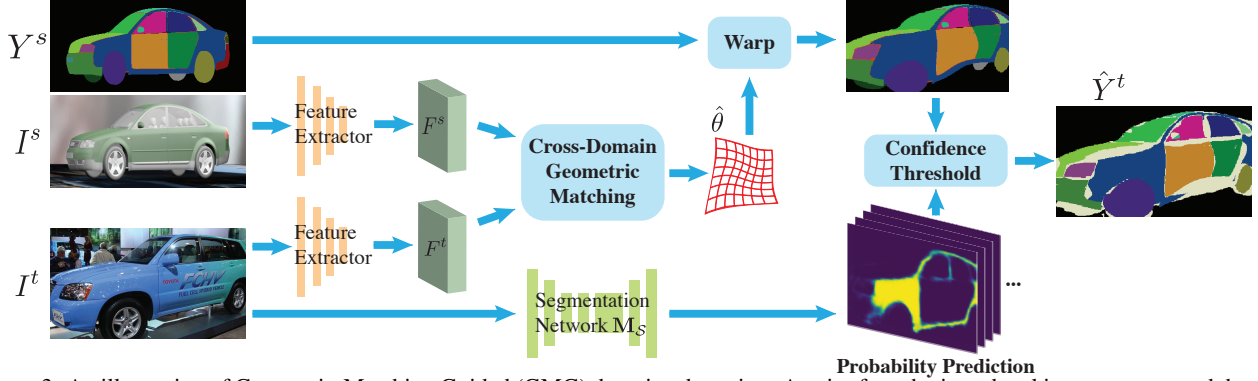


Figure 3: An illustration of Geometric-Matching Guided (GMG) domain adaptation. A pair of synthetic and real images are passed through a feature extractor to get their feature maps, and cross-domain geometric matching is used to estimate a 2-D transformation based on the feature similarities. The transformation is then applied to the segmentation ground-truth of the synthetic image to make it match the parts in the real image. Finally, a confidence threshold is used to filter out unreliable warping results and make high-quality pseudo-labels for the joint training step in unsupervised domain adaptation.

$p_{(i,j)}(c|I^s; w)$  is the predicted category probability based on the model parameters  $w$ .

Generally,  $M^S$  has limited generalization capability and does not perform well on target samples due to domain discrepancy between the real and synthetic data. One common approach in UDA is using  $M^S$  to generate pseudo-labels  $\hat{Y}^t$  on  $I^t$ , which enables a joint training on  $\mathcal{S}_{\text{train}}$  and  $\mathcal{T}_{\text{train}}$  based on the following loss function:

$$\mathcal{L}(\mathcal{S}_{\text{train}}, \mathcal{T}_{\text{train}}) = \sum_{\mathcal{S}_{\text{train}}} \mathcal{L}_{ce}(I^s, Y^s) + \lambda \sum_{\mathcal{T}_{\text{train}}} \mathcal{L}_{ce}(I^t, \hat{Y}^t),$$

where  $\lambda$  balances the loss between source and target domain. The joint training process encourages the learning of domain-invariant features and shared decision boundaries.

Different UDA methods have been proposed to find reliable pseudo-labels  $\hat{Y}^t$  [58, 109, 112], select a relevant subset of  $\mathcal{S}_{\text{train}}$  [42], or add regularization terms and adversarial losses [44, 113] for the joint training process. However, since most of these methods are designed for semantic segmentation, none of them takes advantage of the spatial object structure to predict parts. On the contrary, our proposed Geometric-Matching Guided domain adaptation (GMG) explicitly uses the structural relation between parts to generate pseudo-labels for joint training.

## 4.2. Cross-Domain Geometric Matching

In GMG, we use cross-domain geometric matching to find optimal transformations that can be used to transfer segmentation labels from synthetic to real. Specifically, cross-domain geometric matching aims to find spatial correspondence between a pair of synthetic and real images ( $I^s, I^t$ ). To achieve this, we optimize a transformation function  $\mathbf{W}_\theta$  that matches the two images  $I^s$  and  $I^t$  based on their feature similarities. After the matching, the transformation is applied to transfer the synthetic label  $Y^s$  to the real image  $I^t$  as a pseudo-label  $\hat{Y}^t$ . In the following, we first assume that the input image pair is given and the objects in both images belong to the same prototype and have a sim-

ilar viewpoint. We then discuss how to search such input pairs in an unsupervised manner. Note that cross-domain geometric matching is only used to generate pseudo-labels for the joint-training. At test time, neither a paired input nor a geometric matching is necessary in our framework.

Given ( $I^s, I^t$ ) with similar appearances, we first use CNN convolutional layers to extract their feature maps. The output  $F^s$  and  $F^t$  are  $h \times w \times d$  tensors, which can be interpreted as  $h \times w$  grids of  $d$ -dimensional local features  $f_{(i,j)}^s \in \mathbb{R}^d$ . The similarity between two feature vectors in  $F^s$  and  $F^t$  can be measured by cosine similarity:

$$\phi(f_{(i,j)}^s, f_{(k,l)}^t) = \frac{f_{(i,j)}^s \cdot f_{(k,l)}^t}{\|f_{(i,j)}^s\|_2 \|f_{(k,l)}^t\|_2}.$$

To emphasize the similarities are measured for features sampled from different domains, we use  $(i, j)$  to denote spatial coordinates in  $I^s$ , and  $(k, l)$  for spatial coordinates in  $I^t$ .

We then define a 2D geometric transformation function  $\mathbf{W}_\theta$  so the spatial correspondence between  $I^t$  and  $I^s$  could be found by:

$$\mathbf{W}_\theta : \mathbb{R}^2 \rightarrow \mathbb{R}^2, \quad (k', l') = \mathbf{W}_\theta(k, l),$$

where  $\theta$  denotes the transformation parameters,  $(k', l')$  are the corresponding coordinates of  $(k, l)$  in  $I^s$ .

The quality of a geometric transformation can be measured by the sum of feature similarities at corresponding coordinates:

$$\Phi_\theta(F^s, F^t) = \sum_{(k,l)} \phi(f_{\mathbf{W}_\theta(k,l)}^s, f_{(k,l)}^t),$$

and our goal is to find the best parameters  $\hat{\theta}$  such that:

$$\hat{\theta} = \arg \max_{\theta} \Phi_\theta(F^s, F^t).$$

In practice, we follow Rocco et al. [68] and use a spatial transformer layer [28] to implement the warping, which makes  $\Phi$  differentiable w.r.t  $\theta$ . Note that we just optimize w.r.t. the transformation parameters based on the feature similarities. The CNN backbone is fixed in this step.

**Unsupervised selection of input pairs.** For each real training image  $I^t \in \mathcal{T}_{\text{train}}$ , we perform a grid search over the viewpoint and prototype in the synthetic images and select the best one based on  $\Phi_{\hat{\theta}}$ . More specifically, we first build a pool of prototypical synthetic images by selecting samples from each prototype with 24 diverse viewpoints (i.e., azimuth angles sampled from  $\{0, 30, 60, \dots, 330\}$  and elevation angles sampled from  $\{5, 20\}$ ). Then, we perform geometric matching for  $I^t$  and each  $I^s$  in this pool. The synthetic image that achieves the highest  $\Phi_{\hat{\theta}}$  is selected, and its label is warped to infer the pseudo-label for  $I^t$ .

### 4.3. Confidence Threshold of Pseudo-Labels

Given  $\hat{\theta}$ , we can warp  $Y^s$  to  $I^t$  and use it as pseudo-supervision for joint training. However, the warping results can contain errors due to the variability of the object shapes and 3D pose, or due to a sub-optimal estimation of the transformation parameters. To correct such errors, in GMG, we use the confidence of the prediction provided by the *Source-Only* model  $\mathbf{M}^S$ . Specifically, for spatial coordinates  $(k, l)$  in  $I^t$ , if the corresponding coordinates  $\mathbf{W}_{\hat{\theta}}(k, l)$  in  $I^s$  have ground-truth label  $\bar{c}$ , we use the predicted probability of  $\bar{c}$  by  $\mathbf{M}^S$  at  $(k, l)$  as a confidence score:

$$z_{kl} = p_{(k,l)}(\bar{c}|I^t; \mathbf{w}_S),$$

and threshold  $z_{kl}$  with  $\gamma$  to obtain the final pseudo-label:

$$\hat{y}_{(k,l)}^t = \begin{cases} y_{\mathbf{W}_{\hat{\theta}}(k,l)}^s, & \text{if } z_{kl} > \gamma \\ \mathbf{0}, & \text{otherwise,} \end{cases}$$

where  $\mathbf{0}$  denotes vector with 0 entries everywhere, and is ignored by the cross-entropy loss. Consequently, GMG is able to select high-confidence warping results as pseudo-labels for joint training.

## 5. Experiments

### 5.1. Experimental Settings

**Datasets and evaluation metric.** In all experiments, we use the synthetic samples of the CGPart dataset as the source data. CGPart provides 30000 / 24000 / 24000 / 24000 / 24000 training samples for the object categories car / motorbike / aeroplane / bus / bicycle. We evaluate all methods on two target datasets. In the first set of experiments, **PASCAL3D+** [101] is used as the target dataset, which contains 2763 / 624 / 986 / 548 / 661 unlabeled training images. After training, the domain adaptation models are evaluated on the 200 CGPart real test images which are originally collected from PASCAL3D+ test split. In the second set of experiments, **PascalPart** [9] is used as the target dataset. We pre-process PascalPart data by cropping images to contain single object and filtering out small instances (i.e., shorter edge is less than 50), which leads to 538 / 261 / 266 / 221 / 252 training images, and 520 / 255 / 280 / 229 / 263) test images. Note that the segmentation labels for the PascalPart training images are not used. We train with the dense part labels defined in CGPart first and

then merge the predictions to PascalPart label space during testing. All models are trained and tested on samples belonging to each vehicle category separately. **Mean Intersection over Union (mIoU)** is used as the evaluation metric for the part segmentation task, where IoU is first computed for each part and then averaged over all parts belonging to the corresponding category.

**Baseline methods.** For comparison purposes, we adapt several popular UDA methods from related tasks to object part segmentation. BDL [44], CRST [113], and CAG [109] are all methods proposed for semantic segmentation but follow different strategies: BDL uses cycleGAN to reduce pixel-level domain discrepancy and encourage marginal feature alignment; CRST performs self-training with smoothness regularization; while CAG applies adversarial training as initialization and explores category-aware feature alignment during self-training. In addition, we test CCSSL [58], which is a self-training-based domain adaptation method designed for keypoint detection. CCSSL uses consistency constraints to select reliable pseudo-labels and applies strong data augmentation to improve the model’s generalization capability on real images. The code for all baselines was adapted from the original public repositories and is modified to use the same backbone and input size.

**Implementation details.** We use DeepLabv3+ [8] as the segmentation network for GMG and all baseline methods. The weights are initialized from an ImageNet [13] pre-trained model. We implement our model using Pytorch [62] on two TitanX GPUs. Synthetic training images are resized to have a long edge of 800 pixels while real training images are resized to have a short edge of 224 pixels. We apply random scaling between 0.5 and 2 and random crop of  $513 \times 513$  to all input samples. For evaluation, the real test images are resized to have a short edge of 224. We use batch size equals 12 for training.

The Source-Only model  $\mathbf{M}^S$  is trained for 50 epochs using an SGD optimizer, with momentum set to 0.9 and weight decay equals  $1e - 4$ . The learning rate starts at 0.007 and decreases every epoch using a polynomial scheduler with power 0.9. For geometric matching, we use thin plate spline transformation and take the first four convolutional blocks of an ImageNet [13] pretrained VGG16 network [72] as the feature extractor. The confidence threshold  $\gamma$  is set to the 60th percentile of the scores obtained from all samples in the corresponding category. During joint training, we apply strong augmentations to synthetic images following [58]. The joint training takes 10000 iterations and the learning rate is fixed at  $2.5e - 4$ . We will release the dataset and code after paper acceptance.

### 5.2. Main Results

In Table 2, we report object part segmentation results on the real test images of CGPart. In the header row, the number of parts is denoted in parenthesis next to the category

	car (32)	motorbike (22)	aeroplane (23)	bus (33)	bicycle (18)
Source Only $M^S$	37.19	15.91	13.71	19.43	18.01
CRST [113]	39.35	18.39	13.38	21.03	15.31
BDL [44]	43.60	17.15	16.71	22.95	17.78
CAG [109]	48.97	17.89	16.06	25.74	19.50
CCSSL [58]	49.31	21.87	17.50	24.75	17.27
GMG (Ours)	49.93	23.09	17.89	25.78	19.07
GMG (Ours) w/ vp	53.77	23.28	17.98	26.31	19.09

Table 2: Object part segmentation results (mIoU) on CGPart real test images. The number of parts is denoted in parenthesis next to the category name. “Ours (GMG)” uses unsupervised grid search to find the input pairs, while “Ours (GMG) w/ vp” uses the ground-truth viewpoint of the real training images to reduce the matching error (i.e., grid search over prototype is still necessary).

		car (14)	motorbike (7)	aeroplane (7)	bus (14)	bicycle (8)
Fully-Supervised Learning		40.36	38.08	42.47	34.42	40.57
UDA	Source Only $M^S$	14.24	20.48	23.18	16.02	20.21
	CRST [113]	14.44	24.71	23.04	16.56	22.57
	BDL [44]	19.02	26.89	29.08	17.29	22.45
	CAG [109]	18.39	24.09	28.60	17.12	22.22
	CCSSL [58]	24.23	28.80	32.58	18.59	22.25
	GMG (Ours)	25.61	29.68	33.50	19.30	22.91
GMG (Ours) w/ vp		27.59	30.73	33.98	21.20	23.63

Table 3: Object part segmentation results (mIoU) on PascalPart [9] test images. The number of parts is denoted in parenthesis next to the category name. “Ours (GMG)” uses unsupervised grid search to find the input pairs, while “Ours (GMG) w/ vp” uses the ground-truth viewpoint of the real training images to reduce the matching error (i.e., grid search over prototype is still necessary).

name. The *Source-Only* model  $M^S$  serves as a naïve baseline. We observe that the mIoU is generally low, indicating that the domain shift between CGPart synthetic images and real-world images indeed disturbs the model performance and domain adaptation is necessary. By looking at the overall performance, segmenting parts on *motorbike*, *aeroplane*, and *bicycle* are more challenging since their parts are often small, with irregular shape and self-occlusion, which can also be observed in Figure 1.

Among the baseline methods, CRST only achieves marginal improvement and may even hurt the performance in some cases, implying that simple smoothness regularization is not working very well on this task. Moreover, since our synthetic images are generated with random texture and background, it is hard to reduce pixel-level domain discrepancy, so the results of BDL are not satisfactory either. CAG achieves more improvement on *car* and *bus*, showing category-aware feature alignment may work well on parts with regular shapes and large areas. CCSSL improves most categories, suggesting part segmentation benefits more from consistency constraints and strong augmentations.

Compared with the baselines, GMG achieves very competitive results, outperforming all other methods on *car*, *motorbike*, *aeroplane*, and *bus*. Furthermore, we introduce a variant of GMG, where pseudo-label errors are reduced by using the ground-truth viewpoints of the real training images during geometric matching (i.e., the grid search step only looks for the best prototype). The results from this model are shown in the row “GMG (Ours) w/ vp”. We observe the performance is improved further.

We report object part segmentation results on PascalPart test images in Table 3. For this dataset, we include part segmentation results from a DeepLabv3+ network directly trained from PascalPart labels on real images in a fully-supervised manner. These results can be considered as upper-bound for UDA approaches. Compared with CGPart, the PascalPart test set seems more manageable for some categories since the parts are more coarse-grained with larger sizes. On the other hand, the images in PascalPart are overall with lower quality and contain more truncated or occluded objects, making the segmentation task more challenging. Therefore, the result patterns on different categories are not the same as what we get on CGPart test images. Despite the variations in individual numbers, GMG still outperforms all baseline methods on all categories. Similarly, adding ground-truth viewpoints during training consistently improves GMG performance. This indicates a relevant future research direction. Nevertheless, comparing with the fully-supervised learning results, there is still a large room for improvement.

In Figure 4, we compare object part segmentation results from GMG and the *Source-Only* model. Generally, GMG is better at recognizing the shape and the boundary of parts. GMG can also eliminate wrong predictions that violate the part relations, implying it gains more knowledge about the object structure. On the other hand, GMG is prone to misclassifying small parts, such as the *mirror* of *car* and the *pedal* of *bicycle*, whose labels are harder to be correctly transferred through geometric matching. We consider it as future work to improve GMG performance on smaller parts.

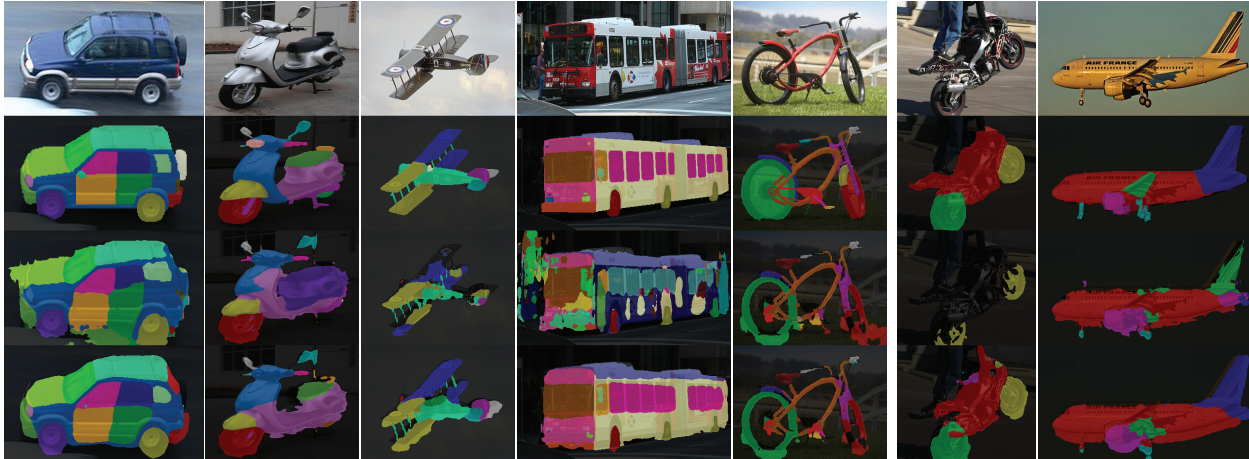


Figure 4: Example part segmentation results on test images from CGPart dataset (column 1-5) and PascalPart dataset [9] (column 6,7). Row 1-4 are real test images, part segmentation ground-truths, *Source-Only* model predictions, and GMG predictions for each case respectively.

### 5.3. Ablation and Model Diagnosis

GMG Variants		car	mtbk	arpl
Source-Only $M^S$		37.19	15.91	13.71
+warped labels	w/o vp	47.84	20.65	16.25
	w/ vp	53.26	21.94	17.22
+conf. thresh.	w/o vp	49.93	23.09	17.89
	w/ vp	53.77	23.28	17.98

Table 4: Ablation study of GMG components. Results are collected from CGPart real test images.

We quantitatively evaluate the improvement introduced by different components of GMG in Table 4. Compared with the *Source-Only* model, a joint training based on directly warped synthetic labels leads to a performance gain by leveraging the pseudo-supervision on real samples. However, this method is more sensitive to misalignment caused by wrong geometric matching. Consequently, we observe a larger performance gap between the models that use viewpoint supervision (*w/ vp*) and those without (*w/o vp*). Applying confidence threshold improves the results in all cases, especially when ground-truth viewpoints are not available for real training samples. In summary, we can observe the effectiveness of both components in our model.

In Figure 5, we evaluate GMG pseudo-label quality and visualize the synthetic samples selected by grid search for the corresponding real images. In the first three examples, the search process successfully finds synthetic images with reasonable prototype and viewpoint. Consequently, geometric matching is performed on image pairs with similar appearances, and GMG successfully generates high-quality pseudo-labels for joint training. In the fourth row, we show a failure case where a wrong (i.e., opposite) viewpoint is selected. Most of the incorrect labels are filtered out by confidence threshold and will not disturb the joint training.

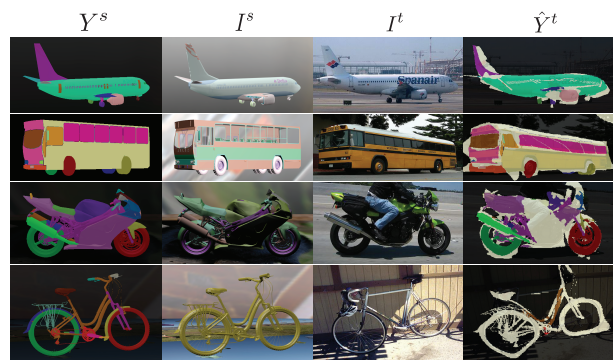


Figure 5: Quality of GMG pseudo-labels. Each row shows the selected source image (2nd column) and its corresponding label (1st column), the target image (3rd column), and the final pseudo-label (4th column). Light yellow color indicates uncertain labels.

## 6. Conclusions

We introduce CGPart, a new part segmentation dataset that provides detailed annotations on 3D CAD models, synthetic images, and real test images. To illustrate the value of CGPart, we use it as a new benchmark for image part segmentation through unsupervised domain adaptation. In our experiments, we adapt several top-performing unsupervised domain adaptation algorithms to part segmentation and observe the results to be not satisfactory. Furthermore, we introduce Geometric-Matching Guided domain adaptation, which leverages the spatial object structure to facilitate the knowledge transfer from the synthetic to the real domain. We believe that our work will motivate more research on part segmentation through domain adaptation.

Moreover, CGPart can be useful for many other computer vision tasks, including, but not limited to, model diagnosis [29, 110], visual analogy reasoning [66, 53], and component-based shape synthesis [30, 50]. We believe CGPart will facilitate and push forward more research using part information and virtual data.

## References

- [1] Hossein Azizpour and Ivan Laptev. Object detection using strongly-supervised deformable part models. In *European Conference on Computer Vision*, pages 836–849, 2012. 1
- [2] Yutong Bai, Qing Liu, Lingxi Xie, Weichao Qiu, Yan Zheng, and Alan L Yuille. Semantic part detection via matching: Learning to generalize to novel viewpoints from limited training data. In *IEEE/CVF International Conference on Computer Vision*, pages 7535–7545, 2019. 3
- [3] Alexander C Berg, Tamara L Berg, and Jitendra Malik. Shape matching and object recognition using low distortion correspondences. In *IEEE Conference on Computer Vision and Pattern Recognition*, volume 1, pages 26–33, 2005. 3
- [4] Qi Cai, Yingwei Pan, Ting Yao, Chenggang Yan, and Tao Mei. Memory matching networks for one-shot image recognition. In *IEEE Conference on Computer Vision and Pattern Recognition*, pages 4080–4088, 2018. 3
- [5] Angel X. Chang, Thomas Funkhouser, Leonidas Guibas, Pat Hanrahan, Qixing Huang, Zimo Li, Silvio Savarese, Manolis Savva, Shuran Song, Hao Su, Jianxiong Xiao, Li Yi, and Fisher Yu. ShapeNet: An Information-Rich 3D Model Repository. Technical Report arXiv:1512.03012 [cs.GR], Stanford University — Princeton University — Toyota Technological Institute at Chicago, 2015. 2, 3
- [6] Wei-Lun Chang, Hui-Po Wang, Wen-Hsiao Peng, and Wei-Chen Chiu. All about structure: Adapting structural information across domains for boosting semantic segmentation. In *IEEE/CVF Conference on Computer Vision and Pattern Recognition*, pages 1900–1909, 2019. 3
- [7] Jianchun Chen, Lingjing Wang, Xiang Li, and Yi Fang. Arbicon-net: Arbitrary continuous geometric transformation networks for image registration. *Advances in Neural Information Processing Systems*, 32:3415–3425, 2019. 3
- [8] Liang-Chieh Chen, Yukun Zhu, George Papandreou, Florian Schroff, and Hartwig Adam. Encoder-decoder with atrous separable convolution for semantic image segmentation. In *ECCV*, 2018. 6
- [9] Xianjie Chen, Roozbeh Mottaghi, Xiaobai Liu, Sanja Fidler, Raquel Urtasun, and Alan Yuille. Detect what you can: Detecting and representing objects using holistic models and body parts. In *IEEE Conference on Computer Vision and Pattern Recognition*, pages 1971–1978, 2014. 1, 2, 3, 4, 6, 7, 8, 15, 16, 18
- [10] Yuhua Chen, Wen Li, Xiaoran Chen, and Luc Van Gool. Learning semantic segmentation from synthetic data: A geometrically guided input-output adaptation approach. In *IEEE/CVF Conference on Computer Vision and Pattern Recognition*, pages 1841–1850, 2019. 3
- [11] Sumit Chopra, Raia Hadsell, and Yann LeCun. Learning a similarity metric discriminatively, with application to face verification. In *IEEE Conference on Computer Vision and Pattern Recognition*, volume 1, pages 539–546, 2005. 3
- [12] Blender Online Community. *Blender - a 3D modelling and rendering package*. Blender Foundation, Stichting Blender Foundation, Amsterdam, 2018. 4, 14
- [13] Jia Deng, Wei Dong, Richard Socher, Li-Jia Li, Kai Li, and Li Fei-Fei. Imagenet: A large-scale hierarchical image database. In *IEEE Conference on Computer Vision and Pattern Recognition*, pages 248–255, 2009. 6
- [14] Jian Dong, Qiang Chen, Xiaohui Shen, Jianchao Yang, and Shuicheng Yan. Towards unified human parsing and pose estimation. In *IEEE Conference on Computer Vision and Pattern Recognition*, pages 843–850, 2014. 1
- [15] Jiahua Dong, Yang Cong, Gan Sun, Yuyang Liu, and Xiaowei Xu. Cscf: Critical semantic-consistent learning for unsupervised domain adaptation. In *European Conference on Computer Vision*, pages 745–762, 2020. 3
- [16] Alexey Dosovitskiy, Philipp Fischer, Eddy Ilg, Philip Hausser, Caner Hazirbas, Vladimir Golkov, Patrick Van Der Smagt, Daniel Cremers, and Thomas Brox. FlowNet: Learning optical flow with convolutional networks. In *IEEE International Conference on Computer Vision*, pages 2758–2766, 2015. 3
- [17] Abhishek Dutta and Andrew Zisserman. The VIA annotation software for images, audio and video. In *ACM International Conference on Multimedia*, 2019. 4, 14
- [18] Hao-Shu Fang, Guansong Lu, Xiaolin Fang, Jianwen Xie, Yu-Wing Tai, and Cewu Lu. Weakly and semi supervised human body part parsing via pose-guided knowledge transfer. In *IEEE Conference on Computer Vision and Pattern Recognition*, pages 70–78, 2018. 3
- [19] Adrien Gaidon, Qiao Wang, Yohann Cabon, and Eleonora Vig. Virtual worlds as proxy for multi-object tracking analysis. In *IEEE Conference on Computer Vision and Pattern Recognition*, pages 4340–4349, 2016. 3
- [20] Ke Gong, Xiaodan Liang, Yicheng Li, Yimin Chen, Ming Yang, and Liang Lin. Instance-level human parsing via part grouping network. In *European Conference on Computer Vision*, pages 770–785, 2018. 1, 2
- [21] Ke Gong, Xiaodan Liang, Dongyu Zhang, Xiaohui Shen, and Liang Lin. Look into person: Self-supervised structure-sensitive learning and a new benchmark for human parsing. In *IEEE Conference on Computer Vision and Pattern Recognition*, pages 932–940, 2017. 1, 3
- [22] Bumsu Ham, Minsu Cho, Cordelia Schmid, and Jean Ponce. Proposal flow: Semantic correspondences from object proposals. *IEEE Transactions on Pattern Analysis and Machine Intelligence*, 40(7):1711–1725, 2017. 3
- [23] Kai Han, Rafael S Rezende, Bumsu Ham, Kwan-Yee K Wong, Minsu Cho, Cordelia Schmid, and Jean Ponce. Snet: Learning semantic correspondence. In *IEEE International Conference on Computer Vision*, pages 1831–1840, 2017. 3
- [24] Ankur Handa, Viorica Patraucean, Vijay Badrinarayanan, Simon Stent, and Roberto Cipolla. Understanding real world indoor scenes with synthetic data. In *IEEE Conference on Computer Vision and Pattern Recognition*, pages 4077–4085, 2016. 3
- [25] Judy Hoffman, Eric Tzeng, Taesung Park, Jun-Yan Zhu, Phillip Isola, Kate Saenko, Alexei Efros, and Trevor Darrell. Cycada: Cycle-consistent adversarial domain adaptation. In *International Conference on Machine Learning*, pages 1989–1998, 2018. 3

- [26] Judy Hoffman, Dequan Wang, Fisher Yu, and Trevor Darrell. Fcns in the wild: Pixel-level adversarial and constraint-based adaptation. *arXiv preprint arXiv:1612.02649*, 2016. [3](#)
- [27] Jiaying Huang, Shijian Lu, Dayan Guan, and Xiaobing Zhang. Contextual-relation consistent domain adaptation for semantic segmentation. In *European Conference on Computer Vision*, pages 705–722, 2020. [3](#)
- [28] Max Jaderberg, Karen Simonyan, Andrew Zisserman, and Koray Kavukcuoglu. Spatial transformer networks. *arXiv preprint arXiv:1506.02025*, 2015. [5](#)
- [29] Justin Johnson, Bharath Hariharan, Laurens Van Der Maaten, Li Fei-Fei, C Lawrence Zitnick, and Ross Girshick. Clevr: A diagnostic dataset for compositional language and elementary visual reasoning. In *IEEE Conference on Computer Vision and Pattern Recognition*, pages 2901–2910, 2017. [3](#), [8](#)
- [30] Evangelos Kalogerakis, Siddhartha Chaudhuri, Daphne Koller, and Vladlen Koltun. A probabilistic model for component-based shape synthesis. *ACM Transactions on Graphics*, 31(4):1–11, 2012. [8](#)
- [31] Mohan S Kankanhalli, Babu M Mehtre, and Ran Kang Wu. Cluster-based color matching for image retrieval. *Pattern Recognition*, 29(4):701–708, 1996. [3](#)
- [32] Khalil Khan, Massimo Mauro, Pierangelo Migliorati, and Riccardo Leonardi. Head pose estimation through multi-class face segmentation. In *IEEE International Conference on Multimedia and Expo*, pages 175–180, 2017. [1](#)
- [33] Jaechul Kim, Ce Liu, Fei Sha, and Kristen Grauman. Deformable spatial pyramid matching for fast dense correspondences. In *IEEE Conference on Computer Vision and Pattern Recognition*, pages 2307–2314, 2013. [3](#)
- [34] Seungryong Kim, Dongbo Min, Bumsub Ham, Sangryul Jeon, Stephen Lin, and Kwanghoon Sohn. Fcss: Fully convolutional self-similarity for dense semantic correspondence. In *IEEE Conference on Computer Vision and Pattern Recognition*, pages 6560–6569, 2017. [3](#)
- [35] Seungryong Kim, Dongbo Min, Stephen Lin, and Kwanghoon Sohn. Dctm: Discrete-continuous transformation matching for semantic flow. In *IEEE International Conference on Computer Vision*, pages 4529–4538, 2017. [3](#)
- [36] Tae Soo Kim, Bohoon Shim, Michael Peven, Weichao Qiu, Alan Yuille, and Gregory D. Hager. Learning from synthetic vehicles. *IEEE International Conference on Image Processing*, 2021. In submission. [4](#), [14](#)
- [37] Bailey Kong, James Supancic, Deva Ramanan, and Charles C Fowlkes. Cross-domain image matching with deep feature maps. *International Journal of Computer Vision*, 127(11):1738–1750, 2019. [3](#)
- [38] Adam Kortylewski, Thomas Albrecht, and Thomas Vetter. Unsupervised footwear impression analysis and retrieval from crime scene data. In *Asian Conference on Computer Vision*, pages 644–658, 2014. [3](#)
- [39] Adam Kortylewski, Bernhard Egger, Andreas Schneider, Thomas Gerig, Andreas Morel-Forster, and Thomas Vetter. Analyzing and reducing the damage of dataset bias to face recognition with synthetic data. In *Proceedings of the IEEE/CVF Conference on Computer Vision and Pattern Recognition Workshops*, pages 0–0, 2019. [3](#)
- [40] Vuong Le, Jonathan Brandt, Zhe Lin, Lubomir Bourdev, and Thomas S Huang. Interactive facial feature localization. In *European Conference on Computer Vision*, pages 679–692, 2012. [1](#)
- [41] Cheng-Han Lee, Ziwei Liu, Lingyun Wu, and Ping Luo. Maskgan: Towards diverse and interactive facial image manipulation. In *IEEE Conference on Computer Vision and Pattern Recognition*, 2020. [1](#)
- [42] Guangrui Li, Guoliang Kang, Wu Liu, Yunchao Wei, and Yi Yang. Content-consistent matching for domain adaptive semantic segmentation. In *European Conference on Computer Vision*, pages 440–456, 2020. [3](#), [5](#)
- [43] Jia Li, James Z Wang, and Gio Wiederhold. Irm: Integrated region matching for image retrieval. In *ACM International Conference on Multimedia*, pages 147–156, 2000. [3](#)
- [44] Yunsheng Li, Lu Yuan, and Nuno Vasconcelos. Bidirectional learning for domain adaptation of semantic segmentation. In *IEEE/CVF Conference on Computer Vision and Pattern Recognition*, pages 6936–6945, 2019. [3](#), [5](#), [6](#), [7](#)
- [45] Xiaodan Liang, Liang Lin, Xiaohui Shen, Jiashi Feng, Shuicheng Yan, and Eric P Xing. Interpretable structure-evolving lstm. In *IEEE Conference on Computer Vision and Pattern Recognition*, pages 1010–1019, 2017. [3](#)
- [46] Xiaodan Liang, Si Liu, Xiaohui Shen, Jianchao Yang, Luqi Liu, Jian Dong, Liang Lin, and Shuicheng Yan. Deep human parsing with active template regression. *IEEE Transactions on Pattern Analysis and Machine Intelligence*, 37(12):2402–2414, 2015. [1](#), [2](#)
- [47] Xiaodan Liang, Xiaohui Shen, Jiashi Feng, Liang Lin, and Shuicheng Yan. Semantic object parsing with graph lstm. In *European Conference on Computer Vision*, pages 125–143, 2016. [3](#)
- [48] Tsung-Yi Lin, Yin Cui, Serge Belongie, and James Hays. Learning deep representations for ground-to-aerial geolocalization. In *IEEE Conference on Computer Vision and Pattern Recognition*, pages 5007–5015, 2015. [3](#)
- [49] Ce Liu, Jenny Yuen, and Antonio Torralba. Sift flow: Dense correspondence across scenes and its applications. *IEEE Transactions on Pattern Analysis and Machine Intelligence*, 33(5):978–994, 2010. [3](#)
- [50] Han Liu, Ulysse Vimont, Michael Wand, Marie-Paule Cani, Stefanie Hahmann, Damien Rohmer, and Niloy J Mitra. Replaceable substructures for efficient part-based modeling. In *Computer Graphics Forum*, volume 34, pages 503–513, 2015. [8](#)
- [51] Xin Liu, Seyran Khademi, and Jan Van Gemert. Cross domain image matching in presence of outliers. In *IEEE International Conference on Computer Vision Workshops*, pages 0–0, 2019. [3](#)
- [52] Mingsheng Long, Yue Cao, Jianmin Wang, and Michael Jordan. Learning transferable features with deep adaptation networks. In *International Conference on Machine Learning*, pages 97–105, 2015. [3](#)

- [53] Hongjing Lu, Qing Liu, Nicholas Ichien, Alan L Yuille, and Keith J Holyoak. Seeing the meaning: Vision meets semantics in solving pictorial analogy problems. In *Annual Conference of the Cognitive Science Society*, 2019. 8
- [54] Wenhao Lu, Xiaochen Lian, and Alan Yuille. Parsing semantic parts of cars using graphical models and segment appearance consistency. *The British Machine Vision Conference*, 2014. 2, 3
- [55] Yawei Luo, Liang Zheng, Tao Guan, Junqing Yu, and Yi Yang. Taking a closer look at domain shift: Category-level adversaries for semantics consistent domain adaptation. In *IEEE/CVF Conference on Computer Vision and Pattern Recognition*, pages 2507–2516, 2019. 3
- [56] Umberto Michieli, Edoardo Borsato, Luca Rossi, and Pietro Zanuttigh. Gmnet: Graph matching network for large scale part semantic segmentation in the wild. In *European Conference on Computer Vision*, pages 397–414, 2020. 3
- [57] Kaichun Mo, Shilin Zhu, Angel X Chang, Li Yi, Subarna Tripathi, Leonidas J Guibas, and Hao Su. Partnet: A large-scale benchmark for fine-grained and hierarchical part-level 3d object understanding. In *IEEE/CVF Conference on Computer Vision and Pattern Recognition*, pages 909–918, 2019. 2
- [58] Jiteng Mu, Weichao Qiu, Gregory D Hager, and Alan L Yuille. Learning from synthetic animals. In *IEEE/CVF Conference on Computer Vision and Pattern Recognition*, pages 12386–12395, 2020. 3, 5, 6, 7
- [59] Zak Murez, Soheil Kolouri, David Kriegman, Ravi Ramamoorthi, and Kyungnam Kim. Image to image translation for domain adaptation. In *IEEE Conference on Computer Vision and Pattern Recognition*, pages 4500–4509, 2018. 3
- [60] Xuecheng Nie, Jiashi Feng, and Shuicheng Yan. Mutual learning to adapt for joint human parsing and pose estimation. In *European Conference on Computer Vision*, pages 502–517, 2018. 3
- [61] David Novotny, Diane Larlus, and Andrea Vedaldi. AnchorNet: A weakly supervised network to learn geometry-sensitive features for semantic matching. In *IEEE Conference on Computer Vision and Pattern Recognition*, pages 5277–5286, 2017. 3
- [62] Adam Paszke, Sam Gross, Francisco Massa, Adam Lerer, James Bradbury, Gregory Chanan, Trevor Killeen, Zeming Lin, Natalia Gimelshein, Luca Antiga, Alban Desmaison, Andreas Kopf, Edward Yang, Zachary DeVito, Martin Raison, Alykhan Tejani, Sasank Chilamkurthy, Benoit Steiner, Lu Fang, Junjie Bai, and Soumith Chintala. Pytorch: An imperative style, high-performance deep learning library. In H. Wallach, H. Larochelle, A. Beygelzimer, F. d’Alché-Buc, E. Fox, and R. Garnett, editors, *Advances in Neural Information Processing Systems 32*, pages 8024–8035. Curran Associates, Inc., 2019. 6
- [63] Vishal M Patel, Raghuraman Gopalan, Ruonan Li, and Rama Chellappa. Visual domain adaptation: A survey of recent advances. *IEEE Signal Processing Magazine*, 32(3):53–69, 2015. 3
- [64] Aayush Prakash, Shaad Boochoon, Mark Brophy, David Acuna, Eric Cameracci, Gavriel State, Omer Shapira, and Stan Birchfield. Structured domain randomization: Bridging the reality gap by context-aware synthetic data. In *International Conference on Robotics and Automation*, pages 7249–7255, 2019. 3, 4
- [65] N Dinesh Reddy, Minh Vo, and Srinivasa G Narasimhan. Carfusion: Combining point tracking and part detection for dynamic 3d reconstruction of vehicles. In *IEEE Conference on Computer Vision and Pattern Recognition*, pages 1906–1915, 2018. 2
- [66] Scott E Reed, Yi Zhang, Yuting Zhang, and Honglak Lee. Deep visual analogy-making. *Advances in Neural Information Processing Systems*, 28:1252–1260, 2015. 8
- [67] Ignacio Rocco, Relja Arandjelovic, and Josef Sivic. Convolutional neural network architecture for geometric matching. In *IEEE Conference on Computer Vision and Pattern Recognition*, pages 6148–6157, 2017. 3
- [68] Ignacio Rocco, Relja Arandjelović, and Josef Sivic. End-to-end weakly-supervised semantic alignment. In *IEEE Conference on Computer Vision and Pattern Recognition*, pages 6917–6925, 2018. 3, 5
- [69] Swami Sankaranarayanan, Yogesh Balaji, Arpit Jain, Ser Nam Lim, and Rama Chellappa. Learning from synthetic data: Addressing domain shift for semantic segmentation. In *IEEE Conference on Computer Vision and Pattern Recognition*, pages 3752–3761, 2018. 3
- [70] Yifei Shi, Pinxin Long, Kai Xu, Hui Huang, and Yueshan Xiong. Data-driven contextual modeling for 3d scene understanding. *Computers & Graphics*, 55:55–67, 2016. 1
- [71] Jamie Shotton, Andrew Fitzgibbon, Mat Cook, Toby Sharp, Mark Finocchio, Richard Moore, Alex Kipman, and Andrew Blake. Real-time human pose recognition in parts from single depth images. In *IEEE Conference on Computer Vision and Pattern Recognition*, pages 1297–1304, 2011. 3
- [72] Karen Simonyan and Andrew Zisserman. Very deep convolutional networks for large-scale image recognition. *arXiv preprint arXiv:1409.1556*, 2014. 6
- [73] Xibin Song, Peng Wang, Dingfu Zhou, Rui Zhu, Chenye Guan, Yuchao Dai, Hao Su, Hongdong Li, and Ruigang Yang. Apollocar3d: A large 3d car instance understanding benchmark for autonomous driving. In *IEEE/CVF Conference on Computer Vision and Pattern Recognition*, pages 5452–5462, 2019. 2
- [74] Yafei Song, Xiaowu Chen, Jia Li, and Qinqing Zhao. Embedding 3d geometric features for rigid object part segmentation. In *IEEE International Conference on Computer Vision*, pages 580–588, 2017. 2, 3
- [75] Michael Stark, Jonathan Krause, Bojan Pepik, David Meger, James J Little, Bernt Schiele, and Daphne Koller. Fine-grained categorization for 3d scene understanding. *International Journal of Robotics Research*, 30(13):1543–1552, 2011. 1
- [76] Baochen Sun and Kate Saenko. Deep coral: Correlation alignment for deep domain adaptation. In *European Conference on Computer Vision*, pages 443–450, 2016. 3
- [77] Jian Sun and Jean Ponce. Learning discriminative part detectors for image classification and cosegmentation. In

- IEEE International Conference on Computer Vision*, pages 3400–3407, 2013. 1
- [78] Tatsunori Tanaii, Sudipta N Sinha, and Yoichi Sato. Joint recovery of dense correspondence and cosegmentation in two images. In *IEEE Conference on Computer Vision and Pattern Recognition*, pages 4246–4255, 2016. 3
- [79] Alexander Thomas, Vittorio Ferrari, Bastian Leibe, Tinne Tuytelaars, and Luc Van Gool. Using recognition to guide a robot’s attention. In *Robotics: Science and Systems*, volume 4, pages 246–253, 2008. 2, 3, 4
- [80] Yicong Tian, Chen Chen, and Mubarak Shah. Cross-view image matching for geo-localization in urban environments. In *IEEE Conference on Computer Vision and Pattern Recognition*, pages 3608–3616, 2017. 3
- [81] Daniel Töpfer, Jens Spehr, Jan Effertz, and Christoph Stiller. Efficient scene understanding for intelligent vehicles using a part-based road representation. In *IEEE Conference on Intelligent Transportation Systems*, pages 65–70, 2013. 1
- [82] Jonathan Tremblay, Aayush Prakash, David Acuna, Mark Brophy, Varun Jampani, Cem Anil, Thang To, Eric Cameracci, Shaad Boochoon, and Stan Birchfield. Training deep networks with synthetic data: Bridging the reality gap by domain randomization. In *IEEE Conference on Computer Vision and Pattern Recognition Workshops*, pages 969–977, 2018. 3, 4
- [83] Yi-Hsuan Tsai, Wei-Chih Hung, Samuel Schulter, Kihyuk Sohn, Ming-Hsuan Yang, and Manmohan Chandraker. Learning to adapt structured output space for semantic segmentation. In *IEEE Conference on Computer Vision and Pattern Recognition*, pages 7472–7481, 2018. 3
- [84] Eric Tzeng, Judy Hoffman, Trevor Darrell, and Kate Saenko. Simultaneous deep transfer across domains and tasks. In *IEEE international conference on computer vision*, pages 4068–4076, 2015. 3
- [85] Eric Tzeng, Judy Hoffman, Ning Zhang, Kate Saenko, and Trevor Darrell. Deep domain confusion: Maximizing for domain invariance. *arXiv preprint arXiv:1412.3474*, 2014. 3
- [86] Nikolai Ufer and Bjorn Ommer. Deep semantic feature matching. In *IEEE Conference on Computer Vision and Pattern Recognition*, pages 6914–6923, 2017. 3
- [87] Gul Varol, Javier Romero, Xavier Martin, Naureen Mahmood, Michael J Black, Ivan Laptev, and Cordelia Schmid. Learning from synthetic humans. In *IEEE Conference on Computer Vision and Pattern Recognition*, pages 109–117, 2017. 3
- [88] Oriol Vinyals, Charles Blundell, Timothy Lillicrap, Koray Kavukcuoglu, and Daan Wierstra. Matching networks for one shot learning. In *International Conference on Neural Information Processing Systems*, pages 3637–3645, 2016. 3
- [89] Tuan-Hung Vu, Himalaya Jain, Maxime Bucher, Matthieu Cord, and Patrick Pérez. Dada: Depth-aware domain adaptation in semantic segmentation. In *IEEE/CVF International Conference on Computer Vision*, pages 7364–7373, 2019. 3
- [90] Jianyu Wang and Alan L Yuille. Semantic part segmentation using compositional model combining shape and appearance. In *IEEE Conference on Computer Vision and Pattern Recognition*, pages 1788–1797, 2015. 2, 3
- [91] Jianyu Wang, Zhishuai Zhang, Cihang Xie, Vittal Premachandran, and Alan Yuille. Unsupervised learning of object semantic parts from internal states of cnns by population encoding. *arXiv preprint arXiv:1511.06855*, 2015. 2
- [92] Peng Wang, Xiaohui Shen, Zhe Lin, Scott Cohen, Brian Price, and Alan L Yuille. Joint object and part segmentation using deep learned potentials. In *IEEE International Conference on Computer Vision*, pages 1573–1581, 2015. 3
- [93] Yang Wang, Duan Tran, Zicheng Liao, and David Forsyth. Discriminative hierarchical part-based models for human parsing and action recognition. *Journal of Machine Learning Research*, 13(10), 2012. 1
- [94] Wikipedia contributors. List of bicycle parts — Wikipedia, the free encyclopedia, 2020. [Online; accessed 9-March-2021]. 3
- [95] Wikipedia contributors. List of auto parts — Wikipedia, the free encyclopedia, 2021. [Online; accessed 9-March-2021]. 3
- [96] Wikipedia contributors. Motorcycle components — Wikipedia, the free encyclopedia, 2021. [Online; accessed 9-March-2021]. 3
- [97] Zuxuan Wu, Xintong Han, Yen-Liang Lin, Mustafa Gokhan Uzunbas, Tom Goldstein, Ser Nam Lim, and Larry S Davis. Dean: Dual channel-wise alignment networks for unsupervised scene adaptation. In *European Conference on Computer Vision (ECCV)*, pages 518–534, 2018. 3
- [98] Fangting Xia, Peng Wang, Liang-Chieh Chen, and Alan L Yuille. Zoom better to see clearer: Human and object parsing with hierarchical auto-zoom net. In *European Conference on Computer Vision*, pages 648–663, 2016. 3
- [99] Fangting Xia, Peng Wang, Xianjie Chen, and Alan L Yuille. Joint multi-person pose estimation and semantic part segmentation. In *IEEE Conference on Computer Vision and Pattern Recognition*, pages 6769–6778, 2017. 3
- [100] Fangting Xia, Jun Zhu, Peng Wang, and Alan Yuille. Pose-guided human parsing by an and/or graph using pose-context features. In *AAAI Conference on Artificial Intelligence*, volume 30, 2016. 3
- [101] Yu Xiang, Roozbeh Mottaghi, and Silvio Savarese. Beyond pascal: A benchmark for 3d object detection in the wild. In *IEEE Winter Conference on Applications of Computer Vision*, pages 75–82, 2014. 1, 2, 4, 6
- [102] Kota Yamaguchi, M Hadi Kiapour, Luis E Ortiz, and Tamara L Berg. Parsing clothing in fashion photographs. In *IEEE Conference on Computer vision and pattern recognition*, pages 3570–3577, 2012. 1, 2
- [103] Fan Yang, Xin Li, Hong Cheng, Jianping Li, and Leiting Chen. Object-aware dense semantic correspondence. In *IEEE Conference on Computer Vision and Pattern Recognition*, pages 2777–2785, 2017. 3
- [104] Yi Yang and Deva Ramanan. Articulated pose estimation with flexible mixtures-of-parts. In *IEEE Conference*

- on *Computer Vision and Pattern Recognition*, pages 1385–1392, 2011. 1
- [105] Li Yi, Vladimir G Kim, Duygu Ceylan, I-Chao Shen, Mengyan Yan, Hao Su, Cewu Lu, Qixing Huang, Alla Sheffer, and Leonidas Guibas. A scalable active framework for region annotation in 3d shape collections. *ACM Transactions on Graphics (ToG)*, 35(6):1–12, 2016. 1, 2, 4
- [106] Amir Roshan Zamir and Mubarak Shah. Image geolocalization based on multiple nearest neighbor feature matching using generalized graphs. *IEEE Transactions on Pattern Analysis and Machine Intelligence*, 36(8):1546–1558, 2014. 3
- [107] Dengsheng Zhang and Guojun Lu. Evaluation of similarity measurement for image retrieval. In *International Conference on Neural Networks and Signal Processing*, volume 2, pages 928–931, 2003. 3
- [108] Ning Zhang, Jeff Donahue, Ross Girshick, and Trevor Darrell. Part-based r-cnns for fine-grained category detection. In *European Conference on Computer Vision*, pages 834–849, 2014. 1
- [109] Qiming Zhang, Jing Zhang, Wei Liu, and Dacheng Tao. Category anchor-guided unsupervised domain adaptation for semantic segmentation. In *Advances in Neural Information Processing Systems*, pages 433–443, 2019. 3, 5, 6, 7
- [110] Yi Zhang, Weichao Qiu, Qi Chen, Xiaolin Hu, and Alan Yuille. Unrealstereo: Controlling hazardous factors to analyze stereo vision. In *IEEE International Conference on 3D Vision (3DV)*, pages 228–237, 2018. 3, 8
- [111] Yifan Zhao, Jia Li, Yu Zhang, and Yonghong Tian. Multi-class part parsing with joint boundary-semantic awareness. In *IEEE/CVF International Conference on Computer Vision*, pages 9177–9186, 2019. 3
- [112] Yang Zou, Zhiding Yu, BVK Kumar, and Jinsong Wang. Unsupervised domain adaptation for semantic segmentation via class-balanced self-training. In *European Conference on Computer Vision*, pages 289–305, 2018. 3, 5
- [113] Yang Zou, Zhiding Yu, Xiaofeng Liu, BVK Kumar, and Jinsong Wang. Confidence regularized self-training. In *IEEE/CVF International Conference on Computer Vision*, pages 5982–5991, 2019. 3, 5, 6, 7

## Appendix A. Supplementary Material

### A.1. Part annotation tool for 3D CAD models

We use the Blender [12] plugin built by Kim et al. [36] to perform per-mesh part labeling on the 3D CAD models. A screen-shot of the software interface is shown in Figure 6, where a group of meshes is selected and labeled as the part *wheel\_front* for the *bicycle* CAD model.

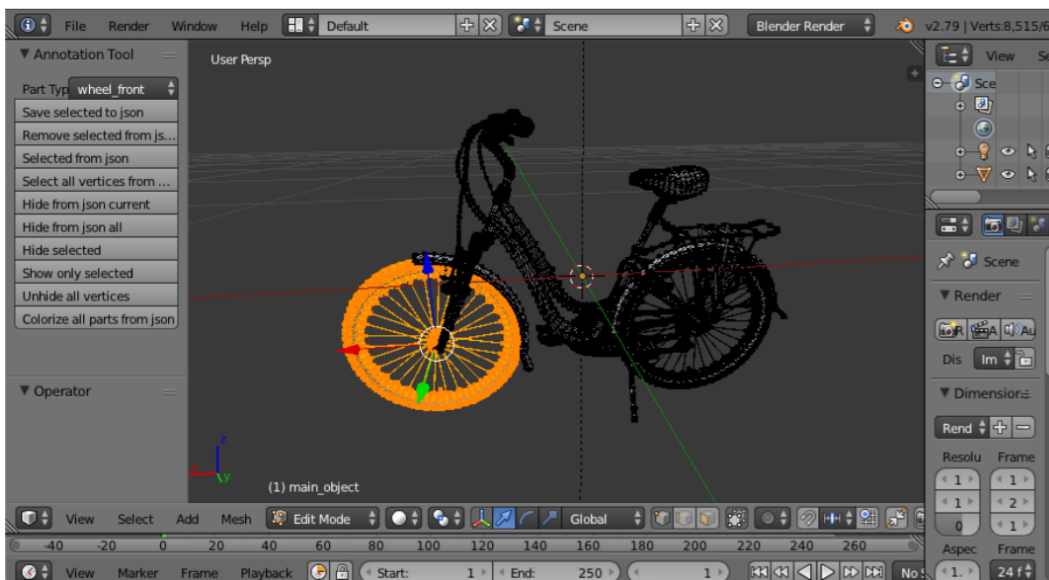


Figure 6: A screenshot of the custom Blender plugin for per-mesh part labeling on 3D CAD models.

### A.2. Part annotation tool for real test images

We use the VGG Image Annotator (VIA) [17] to manually label the parts on the real images. A screen-shot of the annotator interface is shown in Figure 7, where vertices of a polygon are located to define the segmentation mask of the part *cockpit* for the *aeroplane* in this image.

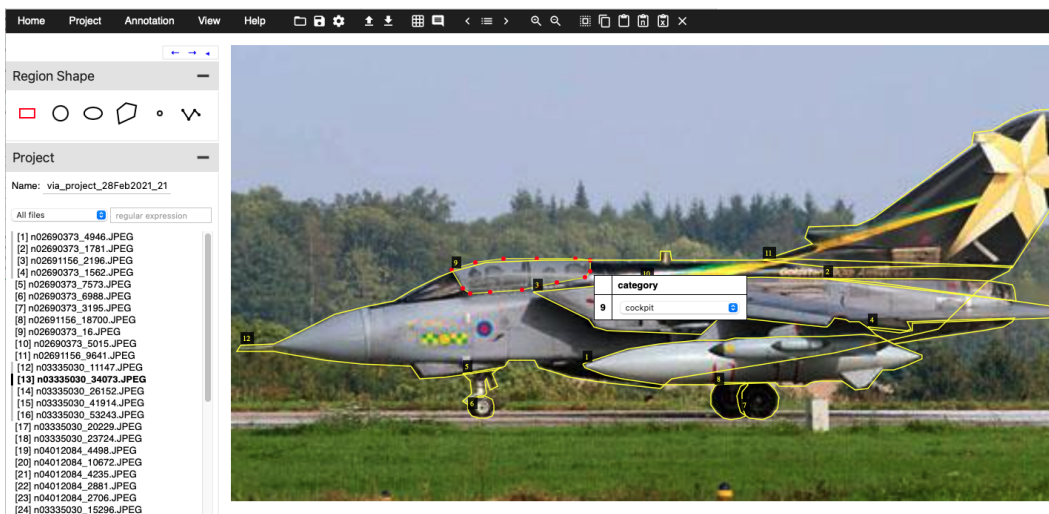


Figure 7: A screenshot of VIA software for manual part annotation on real images.

### A.3. CGPart 3D CAD Models and Part Lists

CGPart is composed of 21 3D CAD models from 5 vehicle categories, each with detailed per-mesh part labeling. Figure 8 shows the all 21 CAD models and their corresponding part annotations. The full lists of parts annotated for each vehicle category can be found in Table 5.

category	part list
car	bumper_back, door_back_left, wheel_back_left, window_back_left, license_plate_back, door_back_right, wheel_back_right, window_back_right, windshield_back, bumper_front, door_front_left, wheel_front_left, window_front_left, license_plate_front, door_front_right, wheel_front_right, window_front_right, windshield_front, hood, frame_left, head_light_left, mirror_left, quarter_window_left, tail_light_left, frame_right, head_light_right, mirror_right, quarter_window_right, tail_light_right, roof, trunk
motorbike	wheel_front, wheel_back, fender_front, fender_back, frame, mirror_left, mirror_right, windscreen, license_plate, seat, seat_back, gas_tank, handle_left, handle_right, headlight, taillight, exhaust_left, exhaust_right, engine, cover_front, cover_body
aeroplane	propeller, cockpit, wing_left, wing_right, fin, tailplane_left, tailplane_right, wheel_front, landing_gear_front, wheel_back_left, landing_gear_back_left, wheel_back_right, landing_gear_back_right, engine_left, engine_right, door_left, door_right, bomb_left, bomb_right, window_left, window_right, body
bus	wheel_front_left, wheel_front_right, wheel_back_left, wheel_back_right, door_front_left, door_front_right, door_mid_left, door_mid_right, door_back_left, door_back_right, window_front_left, window_front_right, window_back_left, window_back_right, licplate_front, licplate_back, windshield_front, windshield_back, head_light_left, head_light_right, tail_light_left, tail_light_right, mirror_left, mirror_right, bumper_front, bumper_back, trunk, roof, frame_front, frame_back, frame_left, frame_right
bicycle	wheel_front, wheel_back, fender_front, fender_back, fork, handle_left, handle_right, saddle, drive_chain, pedal_left, pedal_right, crank_arm_left, crank_arm_right, carrier, rearlight, side_stand, frame

Table 5: Part list for each vehicle category in CGPart

### A.4. More detailed comparisons between CGPart and PascalPart [9]

In Table 6, we list out more details about CGPart and make per-category comparisons with PascalPart [9]. The number of training samples in PascalPart is small, while CGPart provides large-scale synthetic images that is more adequate for deep neural network training. Also, the number of parts in CGPart is 2 to 4 times of the number in PascalPart, indicating CGPart provides more detailed part labeling for each category. In Figure 9, we visualize several examples to compare the part annotations in CGPart and PascalPart. CGPart provides more fine-grained part annotations and these detailedly labeled parts will be more useful for various tasks.

In Figure 10, we further compare the distribution of object azimuth angles, number of parts per image, and number of pixels per part in PascalPart and CGPart real test images. PascalPart is biased to objects in the front-view, while CGPart contains more evenly distributed viewpoints, which results in more evenly distributed part instances. The number of parts per image in PascalPart is 2 to 3 times smaller than CGPart, which agrees with the fact that the number of parts labeled per category in PascalPart is also 2 to 3 times smaller. Moreover, the majority of parts in PascalPart have more than 5000 pixels, while the parts in CGPart have evenly distributed sizes between 100 to 10000 pixels, indicating CGPart is a more challenging dataset for part segmentation.

### A.5. Potential of using CGPart for fully-supervised domain adaptation

Besides unsupervised domain adaptation, CGPart can also be applied to fully-supervised domain adaptation by using PascalPart training labels. Here, we use naïve fine-tuning approach to illustrate the potential. More specifically, we use PascalPart training samples with part labels to train two DeepLabv3+ models: one model is initialized from ImageNet pre-trained weights, and then trained on PascalPart; the other one is first trained for CGPart segmentation, then fine-tuned on PascalPart. The results are shown in Table 7. Using CGPart pre-trained weights consistently improves the final performance

		car	motorbike	aeroplane	bus	bicycle
# of training images	CGPart	(S) 30,000	(S) 24,000	(S) 24,000	(S) 24,000	(S) 24,000
	PascalPart	(R) 538	(R) 261	(R) 266	(R) 221	(R) 252
# of test images	CGParts	(S) 10,000 (R) 40	(S) 8,000 (R) 40	(S) 8,000 (R) 40	(S) 8,000 (R) 40	(S) 8,000 (R) 40
	PascalPart	(R) 520	(R) 255	(R) 280	(R) 229	(R) 263
# of parts	CGParts	31	21	22	32	17
	PascalPart	13	6	6	13	7

Table 6: Per-category comparisons between CGPart and PascalPart [9]. (S) indicates synthetic images, while (R) indicates real images. Note CGPart provides more samples which is more adequate for deep neural network training, and more number of parts per category which makes the segmentation task more challenging.

	Init. from	
	ImageNet	CGPart
car	40.36	41.59
motorbike	38.08	39.42
aeroplane	42.47	44.07
bus	34.42	36.36
bicycle	40.57	41.22

Table 7: Comparison of weight initializations for fully supervised part segmentation in the real image domain. PascalPart [9] training labels are used to train DeepLabv3+ models, and the performance (mIoU) on the test split is shown here. Note if the model is pre-trained on CGPart segmentation task, the final results could be consistently improved by more than 1 point.

on each category for more than 1 point. CGPart pre-training helps the model to start with more meaningful deep features and benefits part segmentation in real image domain even when only naïve fine-tuning is used.

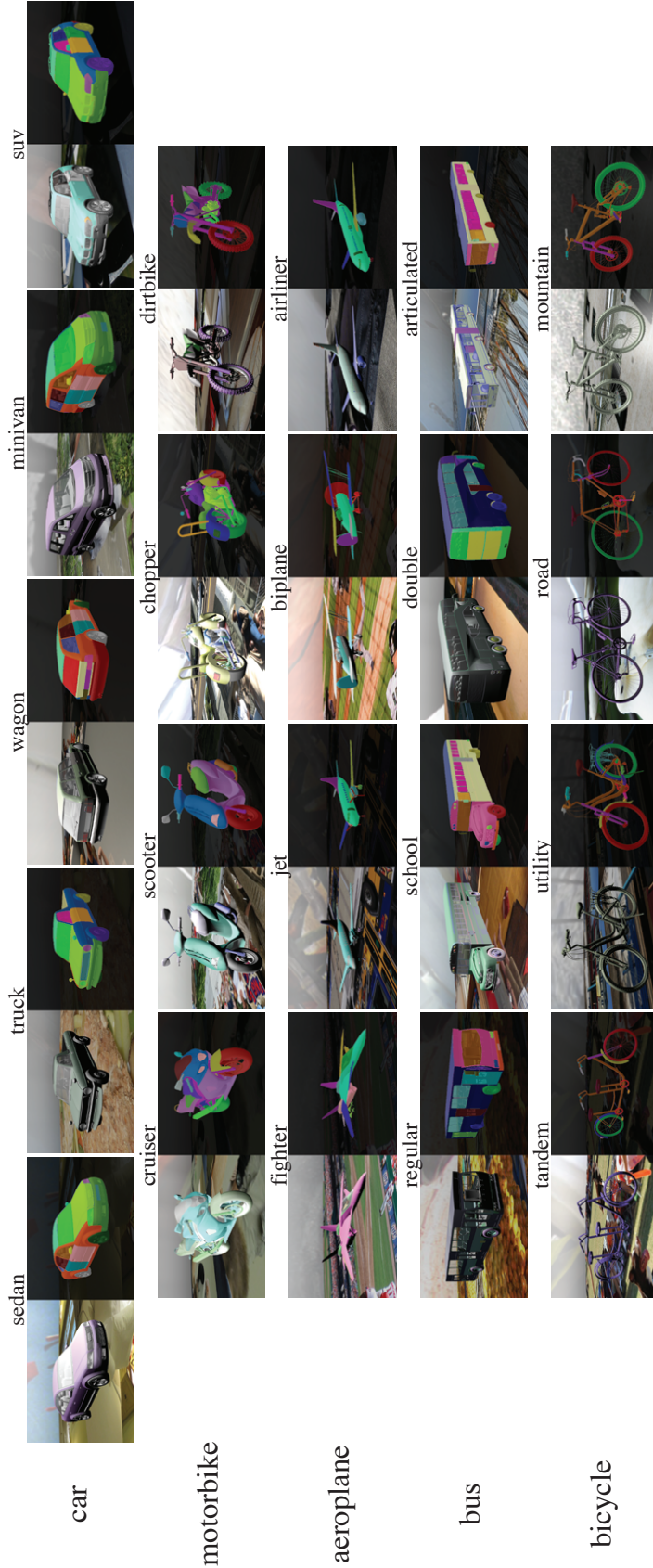


Figure 8: 3D CAD models/sub-categories included in CGPart.

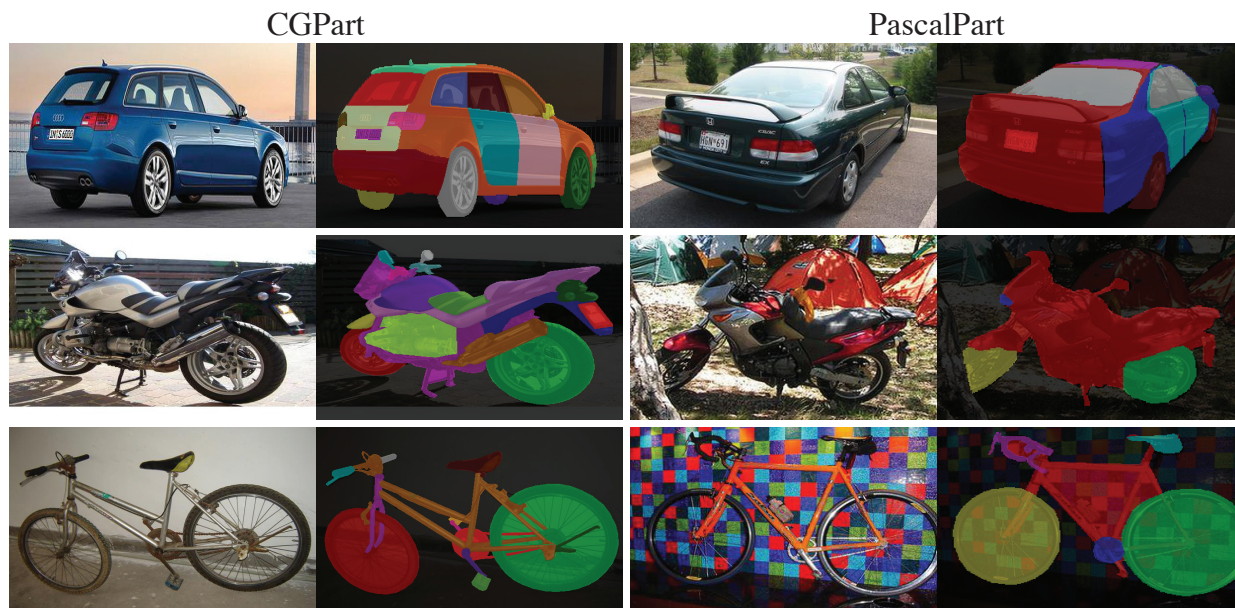


Figure 9: Part annotation comparisons between CGPart and PascalPart [9] dataset. Note CGPart provides more fine-grained part annotations.

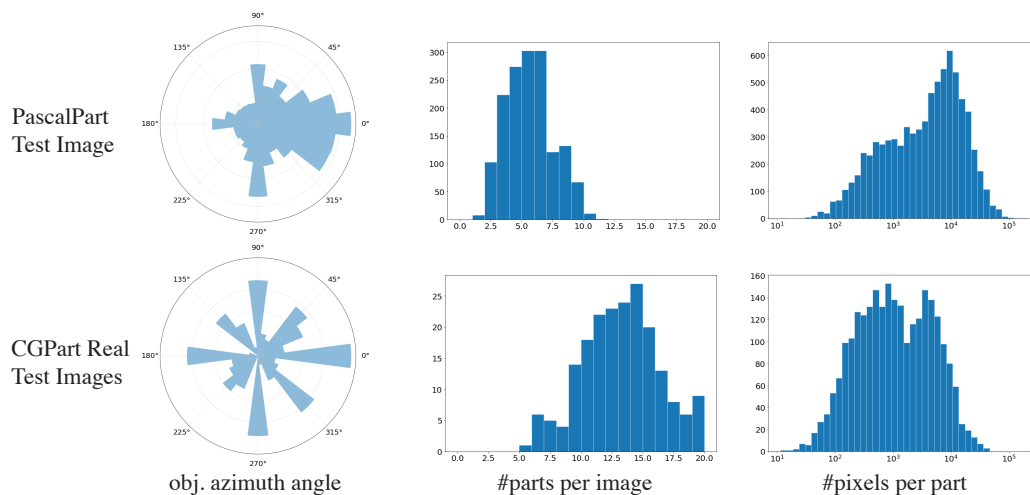


Figure 10: Dataset statistics comparisons between CGPart and PascalPart [9] dataset.